

Influence of non-statistical properties in nuclear structure on emission of prompt fission neutrons

T. Kawano,^{1,*} S. Okumura,^{2,†} A. E. Lovell,¹ I. Stetcu,¹ and P. Talou¹

¹*Los Alamos National Laboratory, Los Alamos, NM 87545, USA*

²*NAPC-Nuclear Data Section, International Atomic Energy Agency, Vienna A-1400, Austria*

(Dated: April 5, 2021)

The Hauser-Feshbach Fission Fragment Decay (HF³D) model is extended to calculate the prompt fission neutron spectrum (PFNS) for the thermal neutron induced fission on ²³⁵U, where the evaporated neutrons from all possible fission fragment pairs are aggregated. By studying model parameter sensitivities on the calculated PFNS, as well as non-statistical behavior of low-lying discrete level spin distribution, we conclude that discrepancies between the aggregation calculation and the experimental PFNS seen at higher neutron emission energies can be attributed to both the primary fission fragment yield distribution and the possible high spin states that are not predicted by the statistical theory of nuclear structure.

PACS numbers: 24.60.-k, 24.60.Dr

I. INTRODUCTION

The nuclear fission process produces a few prompt fission neutrons and a lot of γ -rays to release all the available excitation energies. Generally we assume that the majority of these prompt particles are emitted from two well-separated fission fragments after scission. The neutrons that are evaporated from the two moving fission fragments, which are assumed to be emitted isotropically in the center-of-mass system (CMS) of each fragment, are boosted into the laboratory frame (LAB) [1, 2], and observed as the prompt fission neutron spectrum (PFNS, $\chi(E)$). When a simple evaporation mechanism is assumed, $\epsilon \exp(-\epsilon/T)$, where ϵ is the CMS neutron energy and T is the temperature parameter, the PFNS in the LAB frame is given by the model proposed by Madland and Nix [3]. When a statistical Hauser-Feshbach decay [4] is performed from individual fission fragment pairs [5–8], the aggregated neutron and γ -ray energy spectra — the Hauser-Feshbach Fission Fragment Decay (HF³D) model — should represent direct connection between the statistical decay inside a compound nucleus and experimentally observable data [9–11]. Although such approaches should include the most physics, a long-standing problem remains in the calculated PFNS at higher outgoing neutron energies, namely the energy spectrum on the high energy side (typically above 5 MeV) tends to fall more quickly than experimental data [7].

The problem is primarily due to the energy conservation. An available energy for the evaporating neutron is tightly confined by the fission fragment kinetic energy, the neutron separation energy, and the reaction Q -value for a fixed mass split. The Hauser-Feshbach neutron spectrum will be strictly zero beyond the energetically allowed point, in contrast to the simple evaporation spec-

trum that can go infinity. Due to the requisite energy conservation, the HF³D model often gives too soft shape nevertheless the average energy in the LAB system tends to be consistent with experimental data [12]. It is also reported that the calculated spectrum-average cross sections $\bar{\sigma} = \int \sigma(E)\chi(E)dE$ tend to be smaller than some measured values especially for high threshold energy reactions such as (n,2n) [13]. This has been discussed for a long time by studying model parameter sensitivities, such as the optical model potential, level densities, and γ -ray strength functions, nevertheless a clear explanation has not been made yet.

Many theoretical and experimental studies in the past have confirmed that the fission process produces two fission fragments where high-spin compound states are favorably populated [14–18]. This implies that a compound nucleus decaying by emitting a neutron might be enhanced if the low-lying levels have higher spin I nevertheless the statistical spin distribution predicts a very small probability. The similar phenomenon is reported to the prompt fission γ -ray spectrum (PFGS) by Makii et al. [19]. They argue “non-statistical properties” in nuclear structure, which may enhance γ decay from a high-spin compound state directly to low-lying levels by the E1 transition, if unknown discrete states have somewhat higher spin I than the statistical spin distribution predicts.

In the HF³D model, we take nuclear structure information from the RIPL-3 database [20], which is based on the evaluated nuclear structure data files, ENSDF [21]. When applied to HF³D where we look for nuclear structure properties (excitation energy E_x , spin I , and parity π) of many fission fragments, and this information might be incomplete since many of the fragments are neutron-rich and unstable. To supplement the missing I^π values, we employ the level density formula [22], which implicitly imposes a well-behaved statistical distribution on the low-lying levels. By considering the non-statistical argument in PFGS [19], we envision this could be one of the keys to solve the PFNS issue as well. In this pa-

* kawano@lanl.gov

† S.Okumura@iaea.org

per, we calculate the thermal neutron induced fission on ^{235}U with the HF³D model, and discuss the impact of the non-statistical properties in the nuclear structure on the fission observables.

II. THEORY

A. Hauser-Feshbach fission fragment decay model

The nuclear fission produces a pair of highly excited fission fragments, and they de-excite by emitting several prompt neutrons and γ -rays. The Hauser-Feshbach fission fragment decay (HF³D) model calculates this de-excitation process by the statistical Hauser-Feshbach theory, where the decay probabilities are governed by the neutron and γ -ray transmission coefficients and the level densities at the final states. The neutron transmission coefficients are given by solving the Schrödinger equation for the complex optical potential. We employ the global optical potential parameters of Koning and Delaroche [23]. The Giant Dipole Resonance (GDR) model with the GDR parameters reported in RIPL-3 [20] generates the γ -ray transmission coefficients. A phenomenological model [22, 24] is employed to calculate the nuclear level densities. At low excitation energies, discrete levels given in RIPL-3 are explicitly included instead of the level density model. RIPL-3 often includes some discrete levels to which the excitation energy E_x is experimentally known but its spin I and/or parity π are uncertain. We assign I^π of these states by the Monte Carlo sampling from the spin and parity distributions of

$$R(I, \pi) = \frac{1}{2} \frac{I + 1/2}{\sigma^2} \exp \left\{ -\frac{(I + 1/2)^2}{2\sigma^2} \right\}, \quad (1)$$

where σ^2 is the spin cut-off parameter

$$\sigma^2(E_x) = 0.006945 \sqrt{\frac{U}{a}} A^{5/3} \hbar^2. \quad (2)$$

U is the pairing energy (Δ) corrected excitation energy $U = E_x - \Delta$, a is the energy-dependent level density parameter, and A is the mass number. A 50%-50% partition is assumed for the parity distribution. In the low-excitation energy region, $\sigma^2(E_x)$ is replaced by a constant σ_0^2 estimated from discrete level data. In the fission product mass region, this is approximated by

$$\sigma_0^2 = -3.04 \times 10^{-4} A^2 + 0.141A - 0.265 \hbar^2, \quad (3)$$

and this is connected to Eq. (2) when $\sigma^2(E_x) > \sigma_0^2$.

We perform the statistical Hauser-Feshbach decay calculations for all the produced fission fragments when their yield $Y_P(Z, A)$ is more than 10^{-6} . Typically there are more than 400 fission fragments that are characterized by an initial configuration $P(J, \Pi, E_x)$ — distributions of spin, parity, and excitation energy. The calculated results are averaged by weighting the fission fragment mass and charge distributions. To perform the

five-fold integration over the distributions of $Y_P(Z, A)$ and $P(J, \Pi, E_x)$, the Monte Carlo sampling technique has been utilized [6, 7, 25]. In contrast to the stochastic method, HF³D deterministically performs the numerical integration over these distributions, such that all of the contributing fission fragment pairs are properly included to calculate the averaged quantities. More details are given in our previous publications [9, 10]. Note that there exist more statistical decay codes, which are similar to our model but do not perform the Hauser-Feshbach calculation, see e.g. Refs. [25, 26].

B. Prompt fission neutron spectrum

In the PFNS model by Maldand and Nix [3], either the most probable partition or some representative pairs are included [27, 28]. Alternatively, an aggregation calculation is proposed by Tudora and Hamsch [29]. HF³D is also the aggregation calculation, but the Hauser-Feshbach statistical decay ensures the spin and parity conservation at each of the decay stages.

The CMS neutron spectra $\phi_{L,H}$ from light (L) and heavy (H) fission fragments, which implicitly include all the sequence of multiple neutron emission ($A_{L,H} \rightarrow A_{L,H} - 1 \rightarrow A_{L,H} - 2 \dots$), are normalized to the neutron multiplicity $\nu_{L,H}$,

$$\int dE_x \int d\epsilon \sum_{J\Pi} \phi_{L,H}(J, \Pi, E_x, \epsilon) P_{L,H}(J, \Pi, E_x) = \nu_{L,H}, \quad (4)$$

where the initial configuration $P_{L,H}(J, \Pi, E_x)$ has the normalization

$$\int \sum_{J\Pi} P_{L,H}(J, \Pi, E_x) dE_x = 1. \quad (5)$$

The total kinetic energy TKE is our model input, taken from experimental data, and the fragment kinetic energies $T_{L,H}$ are determined by a simple kinematics

$$T_L = \text{TKE} \frac{A_H}{A_L + A_H}, \quad T_H = \text{TKE} \frac{A_L}{A_L + A_H}. \quad (6)$$

The CMS neutron spectra of light and heavy fragments are transformed into the LAB frame using Feather's formula [1, 2]

$$\psi_{L,H}(E) = \int dE_x \int_{(\sqrt{E}-\sqrt{T_{L,H}})^2}^{(\sqrt{E}+\sqrt{T_{L,H}})^2} d\epsilon \frac{1}{4\sqrt{T_{L,H}\epsilon}} \sum_{J\Pi} \phi_{L,H}(J, \Pi, E_x, \epsilon) P_{L,H}(J, \Pi, E_x). \quad (7)$$

$\psi_{L,H}(E)$ carries the same normalization as Eq. (4), and PFNS is given by averaging $\psi_{L,H}^{(k)}(E)$ weighted by the fission fragment yield y_k , where k is an index for a particular L and H pair

$$\bar{\psi}(E) = \sum_k \left\{ \psi_L^{(k)}(E) + \psi_H^{(k)}(E) \right\} y_k, \quad (8)$$

which is normalized to the average number of prompt fission neutron multiplicity $\bar{\nu}$. Finally, the normalized PFNS is given by

$$\chi(E) = \frac{\bar{\psi}(E)}{\bar{\nu}}. \quad (9)$$

Since the HF³D model was originally developed to calculate the independent and cumulative fission product yields, a very fast algorithm to integrate the excitation energy distribution in Eq. (4) was performed. However, this is not necessarily the best approach for the PFNS calculation, because $T_{L,H}$ depends on the average excitation energy of each fragment, $E_{x,L}$ and $E_{x,H}$. In the PFNS calculation we discretize $P_{L,H}(J, \Pi, E_x)$ into excitation energy bins, and perform the CMS-LAB conversion at each E_x . Detail of the algorithm is given in Appendix . In this technique the CMS-LAB conversion is only exact for the first neutron emission, since we ignore a recoil effect. Even though the multiple neutron emission is treated approximately, this is negligible since typical fission fragment masses are 80 or heavier compared to the neutron mass. Because of numerical integration, the computational time strongly depends on the discretization bin width, and the lowest emission energy is limited to the energy bin size (typically 100 keV). This is in contrast with the Monte Carlo technique, where the emitted neutron energy can be arbitrary [25].

III. RESULT AND DISCUSSION

A. PFNS by the HF³D model

The HF³D model parameters are taken from our previous works [9, 11] for the thermal neutron induced fission on ²³⁵U. The model parameters include the primary fission fragment mass distribution $Y_P(A)$, TKE, the anisothermal parameter R_T [27, 30], a scaling factor f_J applied to the spin distribution of initial configuration, and scaling parameters f_Z and f_N in the odd-even staggering in the charge distribution [31, 32]. $Y_P(A)$ is represented by a few Gaussians, so that the Gaussian width σ_G , the mass shift measured from the symmetric fission Δ_G , and the fraction of each Gaussian component F_G characterize $Y_P(A)$.

We take two sets of the parameters. The first set (prior) included minimum effort of parameter optimization [9], and the second set (posterior) was obtained by adjusting to experimental fission yield data as well as average number of prompt and delayed neutrons [11].

Figure 1 shows the calculated PFNS as ratios to Maxwellian

$$\psi_M(E) = \frac{2}{\sqrt{\pi T^3}} \sqrt{E} \exp\left(-\frac{E}{T}\right), \quad (10)$$

at the temperature T of 1.32 MeV, and compared with experimental data [33–35]. The average energies of these

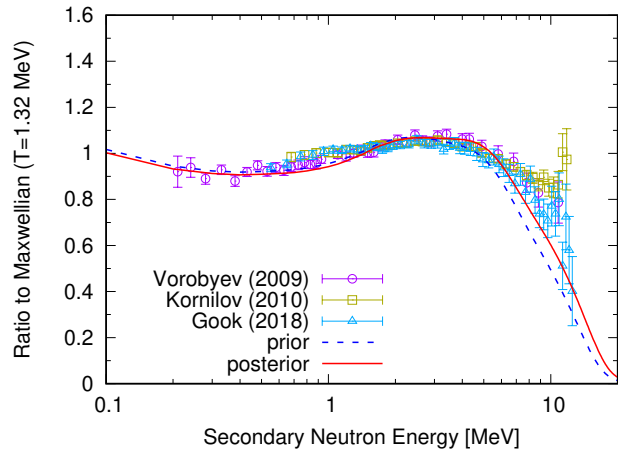


FIG. 1. Comparisons of PFNS predicted by the HF³D model with experimental data. PFNS is shown by ratios to the Maxwellian at the temperature of $T = 1.32$ MeV.

spectra are 1.95 MeV for the prior set and 1.99 for the posterior set. Although the adjustment procedure does not include these PFNS data, the posterior set better reproduces the experimental data up to 7 MeV or so. However, the calculated PFNS still underestimates data at higher outgoing energies.

B. Partial neutron spectrum from fission fragment pairs

Aggregating neutron emission from individual fission fragment pair gives us an insight into which mass partitions give a dominant contribution to PFNS. To study which fission fragment pairs are predominantly causing the difference between the prior and posterior sets in Fig. 1, we decompose the total neutron emission $\bar{\psi}(E)$ for the prior set into each of individual mass split $y_k \psi_{L,H}(E)$, which is shown in Fig. 2. The fission pairs that have the yield y_k of larger than 1% are plotted. The high energy tail in the spectrum comprises of the neutrons from light fragments, because the neutron separation energy, the neutron multiplicity, and fragment kinetic energy are larger. For better visibility, we lump $\psi_{L,H}(E)$ for a fixed mass number A

$$\psi(A_L, E) = \sum_k \{\psi_L(E) + \psi_H(E)\} y_k \delta_{A,A_L}, \quad (11)$$

and this is shown in Fig. 3. The solid curve, which is for $A_L = 102$ and $A_H = 134$, is the highest contribution to the total spectrum above 5 MeV. We noticed the fission fragments near these masses tend to give the harder spectrum tail, and this is clearly shown by the ratio $\psi(A_L, E)/\bar{\psi}(E)$ in Fig. 4. At lower outgoing energies, contributions from each of fission fragment do not show particular characteristics, and they basically follow the

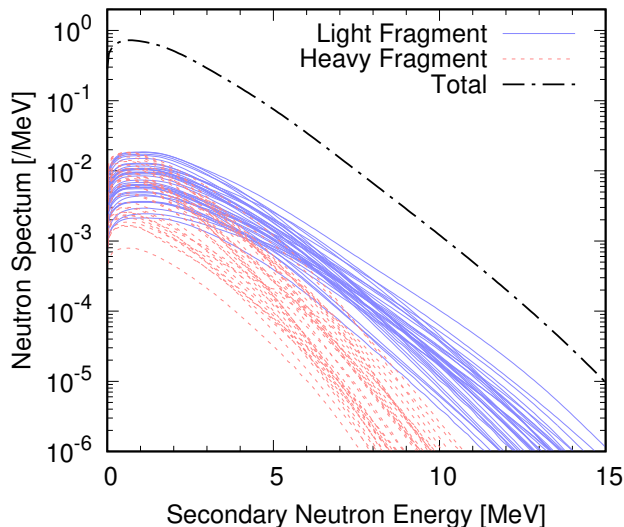


FIG. 2. Individual contribution from each fission fragment to PFNS only for the fragment yield larger than 1%. The light solid curves are from the light fragments, and the dotted curves are from the heavy fragments.

fission fragment yield. However, at higher outgoing energies, some mass regions ($A \sim 87$ and 102) have larger impact on lifting the PFNS tail.

We can see this more clearly by slicing this distribution at the outgoing energy of 10 MeV, and compare with the fission fragment distribution, which is shown in Fig. 5. The posterior $Y_P(A)$, which was obtained by adjusting to some selected fission product yield data, indeed becomes slightly wider distributions. Unexpectedly the fragment yield at $A_L = 102$ decreased after the parameter tuning, and this reduction was compensated by the increase in the outer ($A_L < 90$) and symmetric ($A_L > 102$) regions. This indicates the wider fragment distribution may harden PFNS to some extent, but restricted by reduction in the most sensitive component of $A_L = 102$. We also studied other parameters, R_T , f_J , f_Z , and f_N , as well as TKE. However, they have rather modest sensitivities to PFNS, especially to its shape.

C. Non-statistical properties in discrete levels

The spin distribution in Eq. (1) was derived by an assumption that the distribution of magnetic quantum number m for many particle many hole configurations forms Gaussian with the average of zero [22]. It does not consider any particular properties of nuclear states, such as the collective excitation. Deformed even-even nuclei often show a rotational spectrum (0^+ , 2^+ , 4^+ , \dots), and sometimes we find higher I states at relatively low excitation energies, in contrast to a prediction by the statistical theory. For example, a neutron-rich nucleus ^{102}Zr has very deformed shape ($\beta_2 = 0.36$) [36] and exhibits

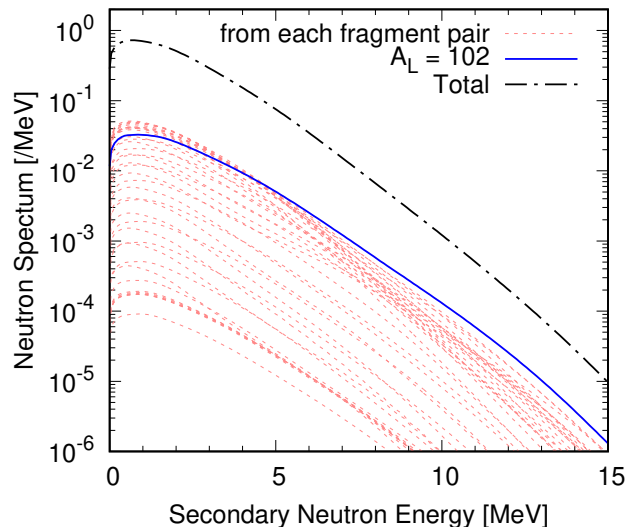


FIG. 3. Partial contributions from each of fission fragment pair to PFNS, where all the same mass splits are lumped.

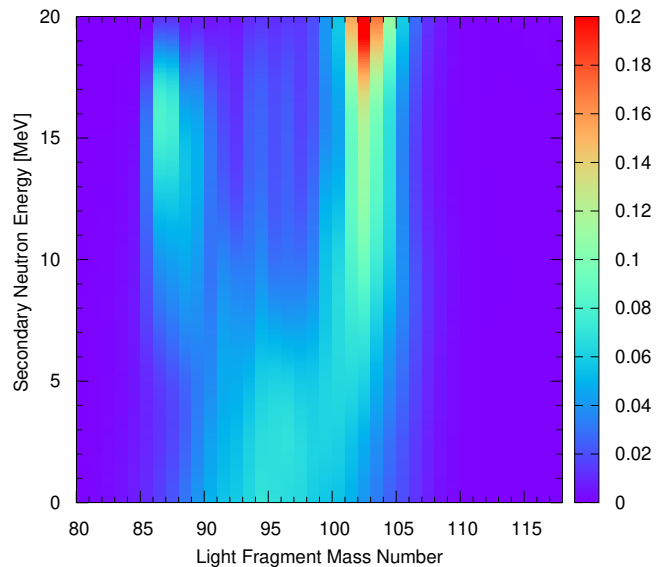


FIG. 4. Partial fission spectra for a fixed A shown as ratios to the total neutron emission, $\psi(A_L, E)/\bar{\psi}(E)$.

the ground state rotational band structure at low energies. However, experimentally known levels in the band are up to the 964-keV (6^+) level.

Because σ^2 as estimated in Eqs. (2) and (3) could have a relatively large uncertainty, and there is no simple way to estimate how the actual spin distribution for a specific nuclide deviates from the statistical prediction unfortunately, we study some overall influence of the non-statistical properties in the low-lying states by adjusting the spin cutoff parameter σ^2 . We conduct this in two approaches; (i) modify unknown I 's that are estimated

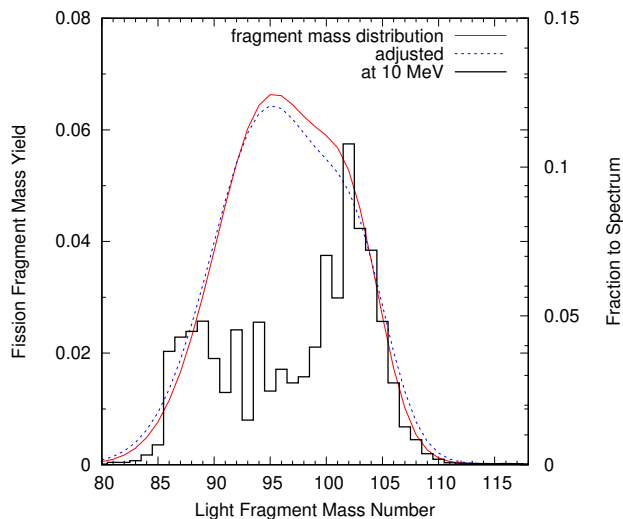


FIG. 5. $\psi(A_L, E)/\bar{\psi}(E)$ for $E = 10$ MeV (right axis), compared with the fission fragment distribution (left axis). Only the light fragment peak is shown.

by σ^2 , and (ii) modify the I -distribution of level density at low excitation energies.

1. Unknown spin of discrete states

We assign a randomly sampled spin to the discrete level whenever I is experimentally unknown (while its excitation energy is known). The sampling is based on Eq. (1), which implies the I -distribution is statistical. To introduce non-statistical fluctuation, we add $4\hbar$ or $6\hbar$ to the assigned spin. Note that this does not change any known I of discrete levels, but only modifies their unknown spin assignment. The result is shown in Fig. 6. We see a significant increase in the high energy tail of PFNS, assuming a non-statistical feature in the discrete levels might be realistic. Although such the non-statistical property may vary nucleus by nucleus, additional $4 - 6\hbar$ to the unknown spins may largely reconcile the discrepancy between the calculated PFNS and experimental data above 7 MeV. These levels relax strong hindrance of high-energy neutron emission from the compound states that also have high spins.

The similar enhancement can be achieved by increasing σ of Eq. (1), and Fig. 6 shows the case when σ is multiplied by 1.5. In this example, we found that ^{94}Rb is one of the dominant contributors causing the bump in the 10 – 15 MeV region. However, this does not suggest any missing high spin states in ^{94}Rb , but just one of many possibilities.

While these modifications changed the PFNS tail notably, increase in the calculated prompt neutron multiplicity $\bar{\nu}$ was less than 0.3%.

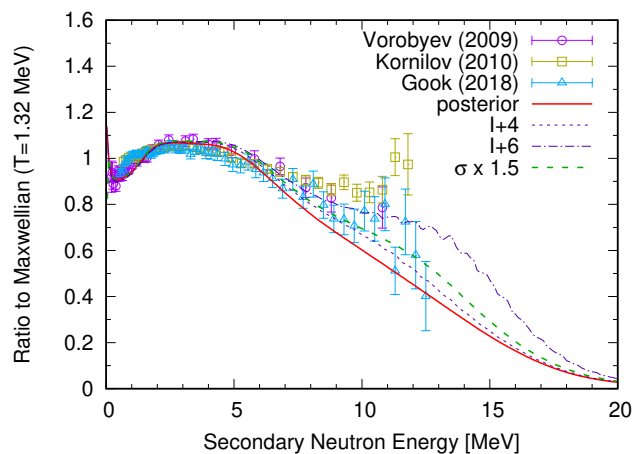


FIG. 6. Comparisons of PFNS predicted by the HF³D model with experimental data, which is shown by ratios to Maxwellian the temperature of $T = 1.32$ MeV. When discrete level spins are unknown, they are increased by $4\hbar$ and $6\hbar$, or sampled from the spin distribution formula where σ is multiplied by 1.5.

2. Spin distribution of level density at low excitation energies

From Eq. (1) the average spin $\langle I \rangle$ is roughly proportional to σ ($\langle I \rangle \simeq 1.2\sigma$), and typical values of σ^2 in the fission product mass region are 10 ($\sigma \sim 3$) or so at low excitation energies; see Eq. (3). When σ is larger than these average values, this also enhances neutron emission from the initially populated compound state. Figure 7 shows how PFNS changes its shape when σ_0 of Eq. (3) is multiplied by 1.1, 1.2, and 1.5. In this case, all of the fission fragments contribute to the shape-change, hence it tends to overshoot the entire experimental data points near 6 MeV, albeit increase in σ lifts the PFNS tail. This is in contrast to Fig. 6, where we increased I only when it is not assigned. This confirms that the deficiency in the model does not reside in the statistically averaged parameters such as the estimated σ^2 but in the incomplete nuclear structure information for some specific nuclei.

The both cases shown above demonstrate that the non-statistical feature in the spin distribution at low excitation energies is sensitive to the tail of PFNS. By following the statistical theory for the level spectrum, extremely high spin states are seldom found at low excitation energies, since the small number of particle-hole configurations hardly couple to high- I . However, the ground state rotational band of even-even nucleus might exhibit $10\hbar$ or higher levels, even though they are not easily observed experimentally. Small non-statistical contributions from each fission fragment would build up in the aggregation calculation, and they finally impact on the PFNS shape. Having said that, it should be noted that the high energy part of PFNS in Figs. 6 and 7 is exaggeratedly plotted by ratios to Maxwellian, where the absolute PFNS varies in

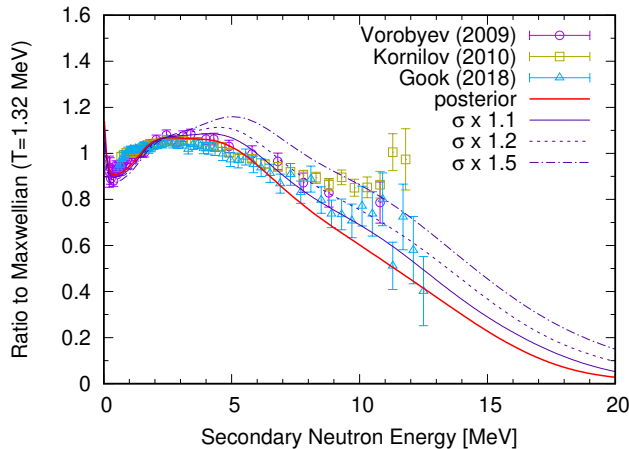


FIG. 7. Comparisons of PFNS predicted by the HF³D model with experimental data. The spin cutoff parameter in the level density formula at low excitation energies is multiplied by 1.1, 1.2, and 1.5.

several orders of magnitude in the MeV region. When we calculate spectrum average cross sections $\bar{\sigma}$ for the high Q -value reactions, such as the (n,2n) reaction, these values would be strongly influenced by assumptions made for uncertain spin of low-lying states. Precise spectroscopic studies on nuclear structure for neutron-rich nuclei are essential to better understand the tail of PFNS.

IV. CONCLUSION

We extended the Hauser-Feshbach Fission Fragment Decay (HF³D) model to calculate the prompt fission neutron spectrum (PFNS). We carefully investigated the long-standing problem of “too soft PFNS” when the aggregated calculation of Hauser-Feshbach neutron spectrum is performed for all the possible fission fragments, and we found two important components in the HF³D model. The primary fission fragment distribution $Y_P(A)$, which is parameterized by several Gaussians, needs to be slightly wider than experimentally reported data. The wider distribution is also supported by other fission observables, such as the cumulative fission product yields, the prompt neutron multiplicity $\bar{\nu}_p$, and the β -delayed $\bar{\nu}_d$. We demonstrated that the primary fragment distribution accounts for the underestimation of PFNS up to 7 MeV. At higher outgoing energies, a possible reason of neutron emission hindrance is a non-statistical nature of the spin distribution in low-lying levels. When some discrete levels to which the spin I is not reliably determined, can have higher I than predicted spin by the statistical model, a high J compound state is able to decay directly to these state by emitting a neutron. This decay process creates the higher energy tail in PFNS, and it may reconcile discrepancies seen in the calculated and experimental spectrum average cross sections.

ACKNOWLEDGMENT

TK thanks Dr. Nishio and Dr. Makii of JAEA for valuable discussions. This work was partially support by both the Nuclear Criticality Safety Program and the Office of Defense Nuclear Nonproliferation Research & Development (DNN R&D), National Nuclear Security Administration, U.S. Department of Energy. This work was carried out under the auspices of the National Nuclear Security Administration of the U.S. Department of Energy at Los Alamos National Laboratory under Contract No. 89233218CNA000001.

-
- [1] N. Feather, *Emission of Neutrons from Moving Fission Fragments*, Tech. Rep. BM-148 (British Mission, 1942).
 - [2] J. Terrell, Fission neutron spectra and nuclear temperatures, *Phys. Rev.* **113**, 527 (1959).
 - [3] D. G. Madland and J. R. Nix, New calculation of prompt fission neutron spectra and average prompt neutron multiplicities, *Nuclear Science and Engineering* **81**, 213 (1982).
 - [4] W. Hauser and H. Feshbach, The inelastic scattering of neutrons, *Phys. Rev.* **87**, 366 (1952).
 - [5] J. C. Browne and F. S. Dietrich, Hauser-Feshbach calculation of the ²⁵²Cf spontaneous-fission neutron spectrum, *Phys. Rev. C* **10**, 2545 (1974).
 - [6] O. Litaize and O. Serot, Investigation of phenomenological models for the Monte Carlo simulation of the prompt fission neutron and γ emission, *Phys. Rev. C* **82**, 054616 (2010).
 - [7] B. Becker, P. Talou, T. Kawano, Y. Danon, and I. Stetcu, Monte Carlo Hauser-Feshbach predictions of prompt fission γ rays: Application to $n_{th} + ^{235}\text{U}$, $n_{th} + ^{239}\text{Pu}$, and $^{252}\text{Cf}(sf)$, *Phys. Rev. C* **87**, 014617 (2013).
 - [8] D. Regnier, O. Litaize, and O. Serot, An improved numerical method to compute neutron/gamma deexcitation cascades starting from a high spin state, *Computer Physics Communications* **201**, 19 (2016).
 - [9] S. Okumura, T. Kawano, P. Jaffke, P. Talou, and S. Chiba, ²³⁵U(n,f) independent fission product yield and isomeric ratio calculated with the statistical Hauser-Feshbach theory, *Journal of Nuclear Science and Technology* **55**, 1009 (2018).
 - [10] A. E. Lovell, T. Kawano, S. Okumura, I. Stetcu, M. R. Mumpower, and P. Talou, Extension of the Hauser-

- Feshbach fission fragment decay model to multi-chance fission, *Phys. Rev. C* **103**, 014615 (2021).
- [11] S. Okumura, T. Kawano, A. Lovell, and T. Yoshida, Energy dependent calculations of fission product, prompt, and delayed neutron yields for neutron induced fission on ^{235}U , ^{238}U , and ^{239}Pu , *Journal of Nuclear Science and Technology* (2021), (under review).
- [12] T. Kawano, P. Talou, I. Stetcu, and M. B. Chadwick, Statistical and evaporation models for the neutron emission energy spectrum in the center-of-mass system from fission fragments, *Nuclear Physics A* **913**, 51 (2013).
- [13] R. Capote, Y.-J. Chen, F.-J. Hamsch, N. Kornilov, J. Lestone, O. Litaize, B. Morillon, D. Neudecker, S. Oberstedt, T. Ohsawa, N. Otuka, V. Pronyaev, A. Saxena, O. Serot, O. Shcherbakov, N.-C. Shu, D. Smith, P. Talou, A. Trkov, A. Tudora, R. Vogt, and A. Vorobyev, Prompt fission neutron spectra of actinides, *Nuclear Data Sheets* **131**, 1 (2016), Special Issue on Nuclear Reaction Data.
- [14] J. B. Wilhelmy, E. Cheifetz, R. C. Jared, S. G. Thompson, H. R. Bowman, and J. O. Rasmussen, Angular momentum of primary products formed in the spontaneous fission of ^{252}Cf , *Phys. Rev. C* **5**, 2041 (1972).
- [15] L. Bonneau, P. Quentin, and I. N. Mikhailov, Scission configurations and their implication in fission-fragment angular momenta, *Phys. Rev. C* **75**, 064313 (2007).
- [16] I. Stetcu, P. Talou, T. Kawano, and M. Jandel, Isomer production ratios and the angular momentum distribution of fission fragments, *Phys. Rev. C* **88**, 044603 (2013).
- [17] G. F. Bertsch, T. Kawano, and L. M. Robledo, Angular momentum of fission fragments, *Phys. Rev. C* **99**, 034603 (2019).
- [18] J. N. Wilson, D. Thisse, M. Lebois, N. Jovančević, D. Gjestvang, R. Canavan, M. Rudigier, D. Étasse, R.-B. Gerst, L. Gaudefroy, E. Adamska, P. Adsley, A. Algora, M. Babo, K. Belvedere, J. Benito, G. Benzoni, A. Blazhev, A. Boso, S. Bottoni, M. Bunce, R. Chakma, N. Cieplicka-Oryńczak, S. Courtin, M. L. Cortés, P. Davies, C. Delafosse, M. Fallot, B. Fornal, L. Fraile, A. Gottardo, V. Guadilla, G. Häfner, K. Hauschild, M. Heine, C. Henrich, I. Homm, F. Ibrahim, L. W. Iskra, P. Ivanov, S. Jazrawi, A. Korgul, P. Koseoglou, T. Kröll, T. Kurtukian-Nieto, L. Le Meur, S. Leoni, J. Ljungvall, A. Lopez-Martens, R. Lozeva, I. Matea, K. Miernik, J. Nemer, S. Oberstedt, W. Paulsen, M. Piersa, Y. Popovitch, C. Porzio, L. Qi, D. Ralet, P. H. Regan, K. Rezykina, V. Sánchez-Tembleque, S. Siem, C. Schmitt, P.-A. Söderström, C. Sürder, G. Tocabens, V. Vedia, D. Verney, N. Warr, B. Wasilewska, J. Wiederhold, M. Yavahchova, F. Zeiser, and S. Ziliani, Angular momentum generation in nuclear fission, *Nature* **590**, 566 (2021).
- [19] H. Makii, K. Nishio, K. Hirose, R. Orlandi, R. LÉguillon, T. Ogawa, T. Soldner, U. Köster, A. Pollitt, F.-J. Hamsch, I. Tsekhanovich, M. Aïche, S. Czajkowski, L. Mathieu, C. M. Petrache, A. Astier, S. Guo, T. Ohtsuki, S. Sekimoto, K. Takamiya, R. J. W. Frost, and T. Kawano, Effects of the nuclear structure of fission fragments on the high-energy prompt fission γ -ray spectrum in $^{235}\text{U}(n_{\text{th}}, f)$, *Phys. Rev. C* **100**, 044610 (2019).
- [20] R. Capote, M. Herman, P. Obložinský, P. G. Young, S. Goriely, T. Belgya, A. V. Ignatyuk, A. J. Koning, S. Hilaire, V. A. Plujko, M. Avrigeanu, O. Bersillon, M. B. Chadwick, T. Fukahori, Z. Ge, Y. Han, S. Kailas, J. Kopecky, V. M. Maslov, G. Reffo, M. Sin, E. S. Soukhovitskii, and P. Talou, RIPL - reference input parameter library for calculation of nuclear reactions and nuclear data evaluations, *Nuclear Data Sheets* **110**, 3107 (2009).
- [21] J. Tuli, Evaluated nuclear structure data file, *Nuclear Instruments and Methods in Physics Research Section A: Accelerators, Spectrometers, Detectors and Associated Equipment* **369**, 506 (1996).
- [22] A. Gilbert and A. G. W. Cameron, A composite nuclear-level density formula with shell corrections, *Can. J. Phys.* **43**, 1446 (1965).
- [23] A. J. Koning and J.-P. Delaroche, Local and global nucleon optical models from 1 keV to 200 MeV, *Nuclear Physics A* **713**, 231 (2003).
- [24] T. Kawano, S. Chiba, and H. Koura, Phenomenological nuclear level densities using the KTUY05 nuclear mass formula for applications off-stability, *Journal of Nuclear Science and Technology* **43**, 1 (2006).
- [25] P. Talou, R. Vogt, J. Randrup, M. E. Rising, S. A. Pozzi, L. Nakae, M. T. Andrews, S. D. Clarke, P. Jaffke, M. Jandel, T. Kawano, M. J. Marcat, K. Meierbachtol, G. Rusev, A. Sood, I. Stetcu, J. Verbeke, and C. Walker, Correlated prompt fission data in transport simulations, *European Physical Journal* **54**, 9 (2018).
- [26] F. Minato, S. Okumura, A. Koning, and T. Kawano, *Implementation of the Hauser-Feshbach theory for Fission Product Yield Evaluation and Fission Modelling*, Tech. Rep. IAEA-NDS-230 (International Atomic Energy Agency, 2020).
- [27] T. Ohsawa, T. Horiguchi, and H. Hayashi, Multimodal analysis of prompt neutron spectra for $^{237}\text{Np}(n,f)$, *Nuclear Physics A* **653**, 17 (1999).
- [28] O. Iwamoto, Systematics of prompt fission neutron spectra, *Journal of Nuclear Science and Technology* **45**, 910 (2008).
- [29] A. Tudora and F.-J. Hamsch, Comprehensive overview of the point-by-point model of prompt emission in fission, *European Physics Journal A* **53**, 159 (2017).
- [30] T. Ohsawa, T. Horiguchi, and M. Mitsuhashi, Multimodal analysis of prompt neutron spectra for $^{238}\text{Pu}(sf)$, $^{240}\text{Pu}(sf)$, $^{242}\text{Pu}(sf)$ and $^{239}\text{Pu}(n_{\text{th}}, f)$, *Nuclear Physics A* **665**, 3 (2000).
- [31] A. C. Wahl, Nuclear-charge distribution and delayed-neutron yields for thermal-neutron-induced fission of ^{235}U , ^{233}U , and ^{239}Pu and for spontaneous fission of ^{252}Cf , *Atomic Data and Nuclear Data Tables* **39**, 1 (1988).
- [32] A. C. Wahl, *Systematics of Fission-Product Yields*, Tech. Rep. LA-13928 (Los Alamos National Laboratory, 2002).
- [33] A. Vorobyev, O. Shcherbakov, and Y. Pleve, Angular and Energy Distributions of Prompt Neutrons from Thermal Neutron-Induced Fission of U-233, U-235 (N,F), ISINN **17**, 60 (2009), international Seminar on Interaction of Neutrons with Nuclei (Dubna, Russia, 2009).
- [34] N. Kornilov, F.-J. Hamsch, I. Fabry, S. Oberstedt, T. Belgya, Z. Kis, L. Szentmiklosi, and S. Simakov, The $^{235}\text{U}(n,f)$ prompt fission neutron spectrum at 100 K input neutron energy, *Nuclear Science and Engineering* **165**, 117 (2010).
- [35] A. Göök, F.-J. Hamsch, S. Oberstedt, and M. Vidali, Prompt neutrons in correlation with fission fragments from $^{235}\text{U}(n, f)$, *Phys. Rev. C* **98**, 044615 (2018).

- [36] P. Möller, J. R. Nix, W. D. Myer, and W. J. Swiatecki, Nuclear ground-state masses and deformations, *Atomic Data and Nuclear Data Tables* **59**, 185 (1995).

Appendix: CMS-LAB conversion in the HF³D model

The HF³D model defines an initial population $P_{L,H}(E_x, J, \Pi)$ in a discretized compound nucleus (CN) with a given energy bin ΔE_x , which is a joint distribution of excitation energy E_x and spin J . The population is normalized as

$$\begin{aligned} & \sum_{J\Pi} \int P_{L,H}(E_x, J, \Pi) dE_x \\ &= \sum_{J\Pi} \frac{1}{2} \int G_{L,H}(E_x) R(J) dE_x \\ &\simeq \sum_{J\Pi} \frac{1}{2} R(J) \sum_k G_{L,H}^{(k)} \Delta E_x = 1, \end{aligned} \quad (\text{A.1})$$

where the excitation energy distributions, $G_{L,H}(E_x)$, for both the light and heavy fragments are represented by a Gaussian

$$G_{L,H}(E_x) = \frac{1}{\sqrt{2\pi}\delta_{L,H}} \exp\left\{-\frac{(E_x - E_{L,H})^2}{2\delta_{L,H}^2}\right\}, \quad (\text{A.2})$$

with the average excitation energy of $E_{L,H}$ and the width of $\delta_{L,H}$. The distribution of spin J is assumed to be proportional to the spin distribution in a level density formula [12],

$$R_{L,H}(J) = \frac{J + 1/2}{f_J^2 \sigma_{L,H}^2(U)} \exp\left\{-\frac{(J + 1/2)^2}{2f_J^2 \sigma_{L,H}^2(U)}\right\}, \quad (\text{A.3})$$

where $\sigma^2(U)$ is the spin cut-off parameter, U is the excitation energy corrected by the pairing energy, and f_J is an adjustable scaling factor. This satisfies the normalization condition of $\sum_J R(J) = 1$. The parity distribution is just 1/2.

Once $P_{L,H}(E_x, J, \Pi)$ is created in a CN, we start a statistical decay calculation (neutron and γ -ray emission by the Hauser-Feshbach theory) from the highest energy all way down to the ground states of all the residual nuclei. Since $P_{L,H}(E_x, J, \Pi)$ is normalized to unity, the sum of the production probabilities of all the residual nuclei also satisfies the normalization. This is equivalent to integrate the initial population over the excitation energy, spin, and parity. The resulting populations of each ground state (or isomeric state if it does not further decay) equal to the independent fission product yield. This is schematically shown in Fig. 8 (a). Although this method simplifies the three-fold integration of E_x , J , and Π , this method has a problem when we apply it to the neutron spectrum in the laboratory system, because the information of fragment kinetic energy is excluded.

When we look into the energy distribution of the prompt fission neutrons, we have to keep track of two fission fragments that are flying away at a given kinetic energy, and the kinetic energy depends on E_x . To do this, as in (b) of Fig. 8, we discretize the excitation energy (the energy-bin is typically 1 MeV, which is wider than ΔE_x of 100 keV or so), and perform the CMS-LAB conversion at each discretized energy-bin so that the kinetic boost is properly included. Although this algorithm yields exactly the same ground state production probabilities as in the case (a), the computational time will be significantly longer.

As a fast algorithm, the method (a) may still be useful for calculating an approximated PFNS. First we calculate the average CMS neutron spectrum, then transform it into the LAB frame by applying the average fragment kinetic energies. However, this procedure tends to yield a harder spectrum and the average energy would be higher by a few percent.

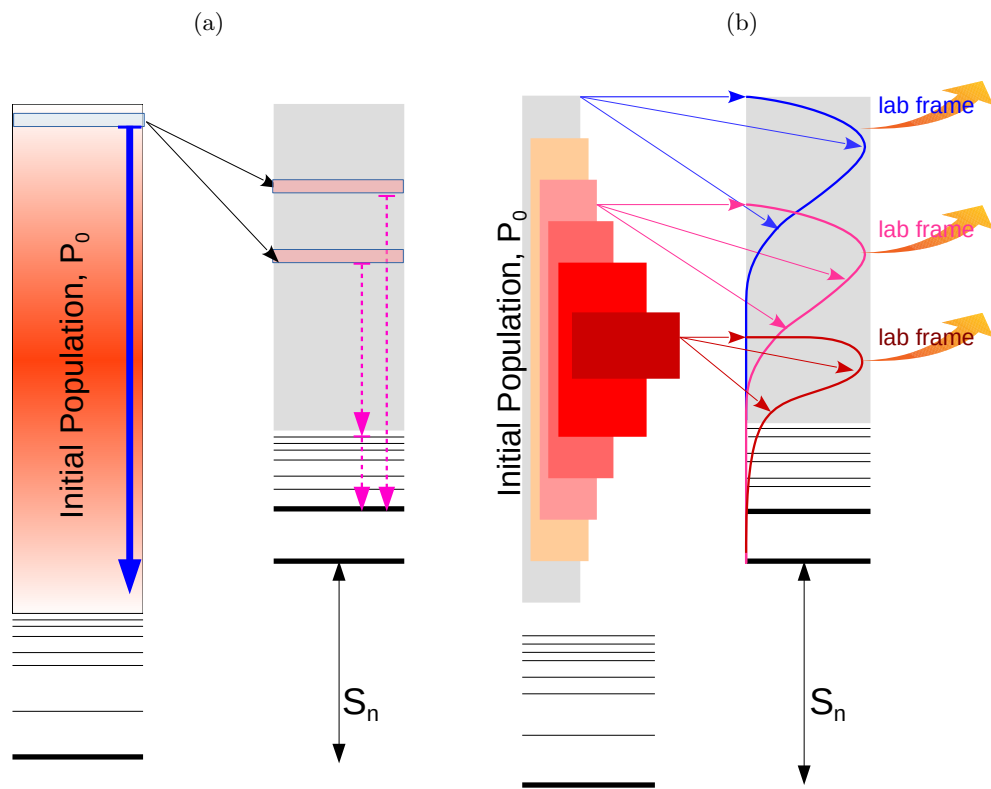


FIG. 8. Scheme of compound decay calculation for (a) the ground state production, and (b) prompt fission neutron spectrum.